Sensor and Simulation Note

Note 404

Suppression of Radiation in Unwanted Directions for a Conical Horn (the Microwave Shade)

D. Robert Smith

Kaman Sciences Corporation
Albuquerque, New Mexico

Carl E. Baum
Robert J. Torres

Phillips Laboratory/WSQ
Kirtland Air Force Base, New Mexico

K. S. H. Lee
F. C. Yang

Kaman Sciences Corporation
Santa Monica, California

17 December 1996

Abstract

This paper considers a new technique for backlobe and sidelobe suppression for fields radiated from a conical horn. It consists of a gradual transition from horn to free space via longitudinal tapered strips, both conducting and resistively loaded. Along with an approximate analysis, data for several configurations are presented, and the designs are compared. Typical reduction of the backlobe is 20 dB, with a slight increase in sidelobe.

1.0 INTRODUCTION

Recently there has been increasing interest in deploying high power (>1 kW) RF sources, both narrowband and wideband, in modern military aircraft for radar, EW, and other applications. Whenever high power RF emitters are installed on an aircraft there is the concern of possible electromagnetic interference (EMI) with other on-board electronic equipment. Modern military aircraft use sophisticated and complex electronic equipment for computers, flight control, navigation, communications, etc. While interference with on-board receivers operating within the same or nearby frequency bands is of particular concern, "backdoor" coupling via unintentional paths onto low-level signal lines inside interior compartments can also be a problem. This paper addresses several ways to minimize the sidelobe and backlobe radiation from a horn antenna on an aircraft and thereby minimize the undesired coupling to other aircraft electronic systems.

Horns are often the antenna of choice for high power narrowband sources because of their power handling capability, simplicity, and relatively compact size. TEM horns are frequently used for wideband antennas. Diffraction from the edges of a horn antenna scatters RF energy into side- and back-lobes, where it may couple onto the aircraft skin and into receiving antennas and interior compartments housing electronic equipment. Although hardening of specific equipment on the aircraft on a case-by-case basis may still be necessary, a practical, generic "first step" is to try to reduce the RF energy radiated in the side and backlobes of the horn. There are at least three partially effective approaches which may be implemented individually or in combination:

1.) Modify the horn edges to minimize the diffraction into the side- and back-lobes.

2.) Redirect diffracted waves away from the side- and back-lobes and into the forward direction instead.

3.) Use RF absorber material around the sides of the horn to absorb side- and back-lobe emissions.

Each of these techniques has advantages and limitations which will be addressed in a qualitative way in the next section. We will consider each technique in the context of reduction of side- and back-lobe emission from a linearly- or circularly- polarized conical horn antenna driven in the TE_{11} circular waveguide mode. In Section 3 we will present a detailed analysis of a backlobe redirecting device which utilizes an array of rectangular notches parallel to the horn axis. Finally, in Section 4 we present conclusions and recommendations for other backlobe/ sidelobe suppressor designs utilizing some of the results of this study.

2.0 APPROACHES

In this section we examine in a qualitative way the three general design approaches listed in Section 1 for reducing side- and back- lobes from a horn antenna:

2.1 ANTENNA EDGE DESIGN TO MINIMIZE DIFFRACTION

The fields radiated by a conical horn originate from two sources (not precisely separable):

- the aperture fields at the horn opening, and
- diffraction from the edge of the horn, which defines the aperture.

For horn antennas with aperture dimensions greater than several wavelengths at the operating frequency, diffraction from the horn edge is a major contributor to the sidelobes and backlobes. One approach to reducing the backlobe emission from a horn is to design the horn edge structure in such a way as to minimize the diffracted energy in the side- and back-lobes.

The edge-diffracted electric field can be expressed as:

$$\mathbf{E}^d = \mathbf{E}^i \bullet \mathbf{D} f_s e^{-jks} \tag{2.1}$$

where $\mathbf{E}^i$ is the incident field at the diffraction point, $\mathbf{D}$ is the dyadic diffraction coefficient, f_s is the diffraction field spreading factor, $k = 2\pi f/c$ is the wavenumber, f is the frequency, c is the speed of light, and s is the distance between the diffraction and field points. Thus, reduction of the diffracted fields can be accomplished by

1. reduction of the incident field intensity $\mathbf{E}^i$ at the diffraction point,
2. reduction of $\mathbf{D}f_s$, the product of the dyadic diffraction coefficient and the diffraction field spreading factor.

Dual Mode and Corrugated Horns

Dual mode horns [1] and corrugated horns [2] reduce the diffracted fields by reducing the field intensity incident on the aperture edges. A dual mode horn utilizes a discontinuity at a position within the horn where two modes can exist. The horn length is adjusted until the total field produced by superposition of the two modes at the aperture edges is minimized. Improved pattern performance over about a 10% frequency band can be achieved.

A corrugated horn uses specially designed corrugated surfaces on the interior walls of the horn to force the RF energy off the surface near the aperture edges. With a horn of sufficient length, improved pattern performance can be expected over nearly a 2:1 bandwidth [2]. However, the corrugations introduce additional reflections which modify the horn impedance, but, with proper design, VSWR's of less than 1.2 over a 1.7:1 frequency band can be obtained [2].

Aperture Matching

Burnside [3] has reported a novel horn design which reduces edge diffraction, not by reducing the incident fields, but by reducing the magnitude of the aperture diffraction coefficient. This is accomplished with aperture curved surfaces which form matching sections between the horn modes and free space radiation. Burnside was able to reduce the E-plane pattern sidelobe of a pyramidal horn by 10-15 dB with this approach. Although the curved surfaces analyzed by Burnside were elliptic cylinder sections, he states that they can be "arbitrary smooth convex shapes."

2.2 A DEVICE WHICH REDIRECTS DIFFRACTED WAVES FORWARD

According to Keller's law of diffraction [5], a ray incident upon an edge produces infinitely many diffracted rays, all of which lie on the surface of a cone having as its axis the tangent to the edge at the point of diffraction. The half angle of the cone is just the angle between the incident ray and the edge, analogous to the geometrical optics law for reflection of rays from a surface. For a conical horn aperture the incident rays are perpendicular to the edge, and the "cone" of diffracted rays becomes a plane perpendicular to the edge. As a result, backlobe fields from a conical horn have a circumferential dependence similar to that of the fields inside the horn incident upon the horn edge. Thus, for a horn excited by a TE_{11} mode, the back-diffracted radiation is strong in the E-plane and weak in the H-plane.

Staggered Length Tapered Strips

Figure 2.1 shows a device consisting of tapered conducting strips separated by tapered gaps which, when attached to the horn edge, can be effective in redirecting energy which would otherwise have been diffracted into the backlobe. A simple way of looking at such a structure is to treat it as a device for gradually transitioning from the horn to free space. The leakage through the horn wall is initially small, building up gradually until the gaps or slots have completely removed the horn boundary. If the wave is propagating in the forward direction in the slots, then one expects the radiation to be predominantly forward, as desired. However, the ending of the strips (as cone tips) may produce a

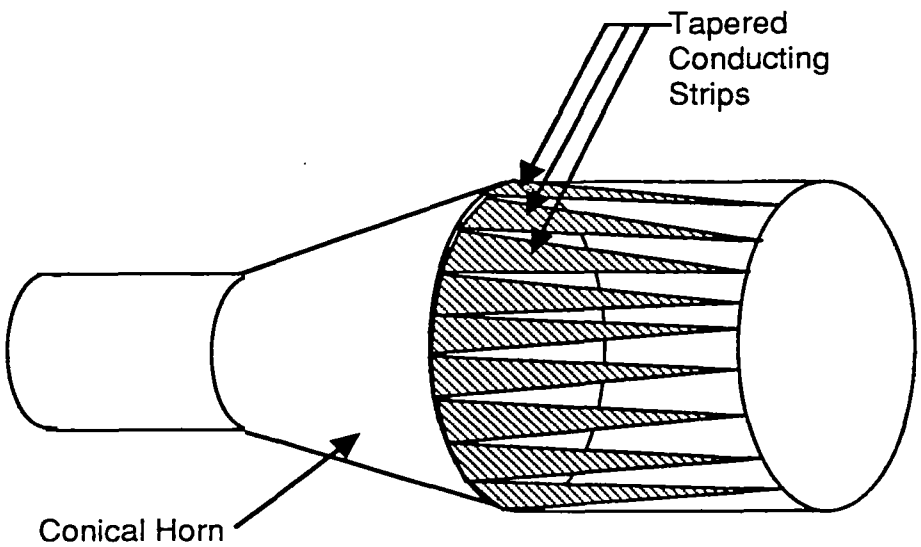

Figure 2.1. Backlobe reduction with tapered conducting strips.

significant reflection. The effect of such reflections can be reduced as indicated in fig. 2.2 by staggering (alternating) the positions (lengths) of the tips by $\lambda/4$, and similarly for the positions (depths) of the slot beginnings (complementary cone tips). In the backwards direction (along the outside of the cone) the scattering (and hence the exterior surface current) should approximately cancel, achieving the desired result. However, for positions away from the horn surface (e.g., in the broadside direction) the cancellation effect can be significantly reduced. Also, it is, in general, not sufficient to consider only paths from two adjacent tips, or two adjacent slot tips, since diffraction from all tips (and from elsewhere along the slots) can contribute to the field at the observation point.

Effect of Loading Tapered Conductors with Lossy Material

The above discussions have assumed a pure traveling wave inside the tapered strip cage attached to the horn, implying that reflections at the various discontinuities are so small that the standing wave component is negligible. This assumption is probably justified, since the horn by its design provides a gradual transition from the waveguide to free space, and the tapered conducting strips should only result in a better match. There will, however, still be some reflection at the tips of the conductors and slots. The effect of these reflections will be enhanced when the strip length is equal to a multiple of a half-wavelength (determined by the phase velocity inside the strip cage). The resulting standing wave patterns tend to create stronger side-lobes and back-lobes at those frequencies.

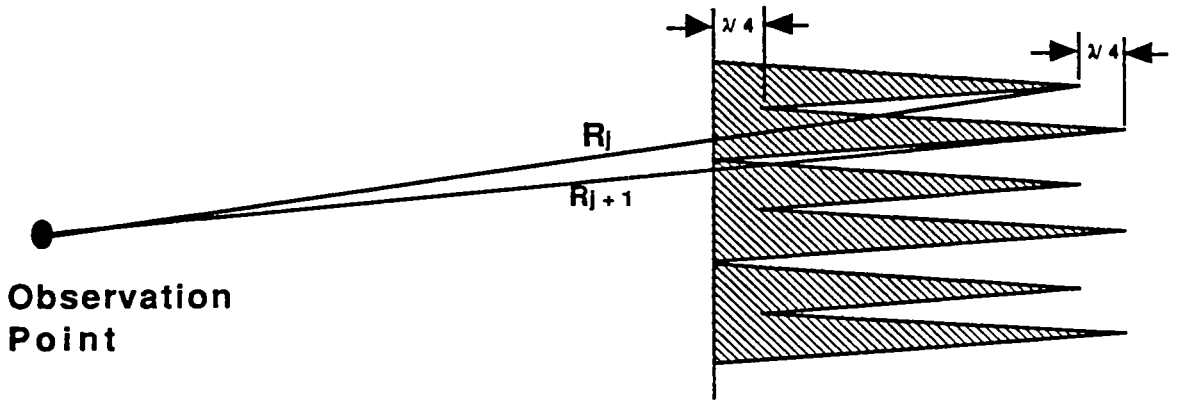

Figure 2.2. Staggered length array of tapered conductors and slots.

Loading the conductors and/or the slots in a manner similar to that used for wire antennas [7] is one means of reducing the standing wave fields inside the tapered conductor cage. One can write down a general equation for the electric current on the conductor (or the magnetic current in the slot) with an unspecified loading function, which can then be determined given the desired electric or magnetic traveling wave current. However, this usually results in a loading function which is difficult if not impossible to synthesize in practice. Figure 2.3 shows a possible implementation of such a loading. The tapered conductor strips overlay strips of lossy material such as carbon impregnated foam or graphite epoxy as shown.

Figure 2.4 shows experimental results obtained with a cylindrical cage of strip pattern similar to that shown in Fig. 2.3 attached with aluminum tape to a 50 cm diameter conical horn antenna. The horn was radiating in a linearly polarized TE_{11} mode. The graph plots the scattering parameter S_{21} measured with a vector network analyzer, where port 1 of the network analyzer was connected to the horn, and port 2 was connected to a surface B-dot sensor attached to the outer surface of a conducting tube. The horn was positioned inside the tube with the horn aperture extending 20 cm beyond the edge of the tube. While this was not intended to be a far-field measurement, it does provide a comparison of the backlobe radiation with and without the cage. The cage consisted of "long" and "short", 2.5cm wide tapered aluminum strips. The long strips were 46cm in length and were separated by short strips of varying lengths selected to be 1/4 wavelength shorter than the long strips for frequencies ranging from 900 to 1200 MHz in 50 MHz increments. The aluminum strips overlaid tapered strips of carbon paper of surface resistance 5000 ohms per square, similar to that shown in Figure 2.3. The reader will observe that in the range around 1 GHz, the "backlobe" is significantly reduced, as expected.

Subsequent tests with a similar cage constructed without the carbon paper strips yielded identical results, indicating that the 5000 ohms/square carbon paper was not a major contributor to the reduction

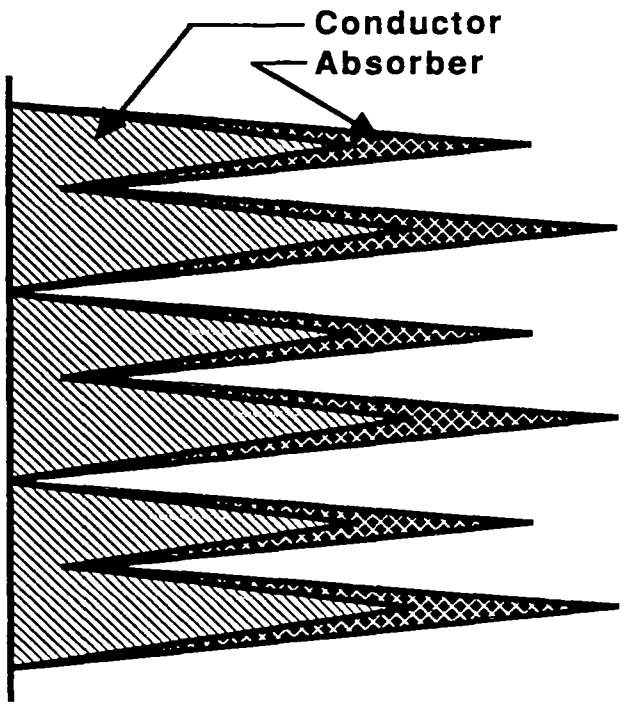

Figure 2.3. Tapered conductors and slots loaded with absorber material.

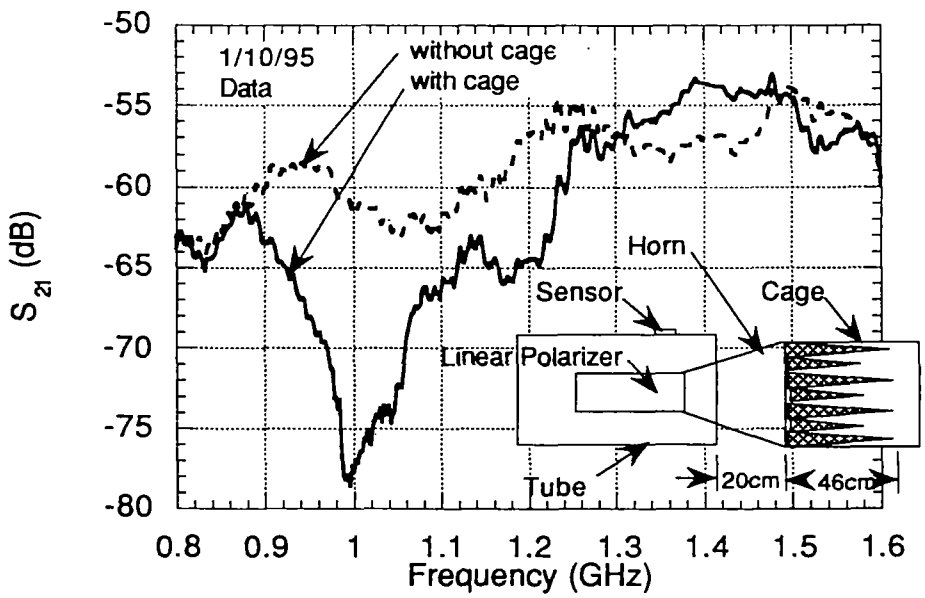

Figure 2.4. Tube surface currents measured with and without cage consisting of tapered conducting and absorbing strips.

in backlobe emission, probably because the sheet resistance was too large and should be reduced to the order of the wave impedance of free space (≃377 Ω). Figure 2.5 shows a similar plot with and without a cage consisting of 30 cm long by 2.5 cm wide tapered strips of graphite epoxy. A graphite epoxy paste was mixed from epoxy and hardener materials, applied to the tapered strip pattern with a spatula to a thickness of approximately 2 mm, and allowed to dry. The surface resistivity of the hardened material was not measured. The horn was excited in a circularly polarized TE_{11} mode. Note the 10 - 15 dB reduction in signal across the band with occasional dips of 25 dB.

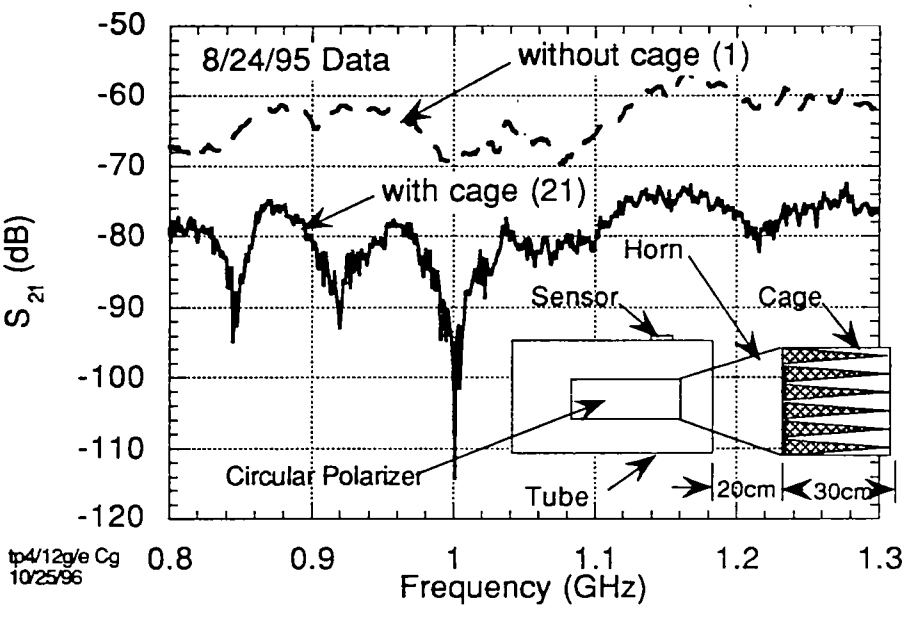

Figure 2.5. Tube surface currents measured with and without cage consisting of 30 cm long, tapered graphite epoxy strips.

Scattering Sources

The fields from the modified horn configuration shown in figs. 2.1, 2.2, and 2.3 have the following sources:

- the aperture fields at the new front opening,
- the diffracted fields from the edges of the strips,
- the diffracted fields from the tips of the strips and slots,
- the fields leaking through the tapered slots.

Since the angles between the incident rays and the tapered strip edges are very small, the Keller's cones of rays diffracted from the tapered strip edges are predominantly in the forward direction. Thus the tapered strip device, which is electrically in contact with the horn edge, effectively changes the shape of the horn edge from one in which the incident rays encounter it at normal incidence (resulting in back - diffraction) to one in which the rays are incident at almost grazing incidence, with no diffracted rays in the backlobe direction.

However, there is still diffraction from the tips of the tapered strips. Unlike edge diffraction, rays diffracted from tips occupy a solid angle of 4π steradians about the tip. Since the wavefronts are essentially spherical, the tip diffracted fields decay as r^{-1} compared to $r^{-1/2}$ for edge diffracted fields. The net effect of tip and edge diffraction is a reduction in backlobes resulting from substitution of the weaker tip diffraction for diffraction from the horn edge.

Field Leakage Through Tapered Slots

There is also some field leakage through the tapered slots which can be analyzed assuming traveling wave magnetic currents in the slot apertures. The traveling wave assumption is valid since the reflection at the ends of the slot are small, because the horn is designed to be an efficient radiator; reflection from the horn edge is already very small even without the tapered conducting strips attached. The addition of the tapered elements should provide an even more gradual transition to free space, resulting in a better match than with the horn alone.

For TE_{11} excitation the phase velocity of the traveling wave is

$$v_{ph} = \frac{c}{p} = \frac{c}{\sqrt{1-\left(\frac{\lambda}{\lambda_c}\right)^2}} \tag{2.2}$$

where $\lambda = 2\pi/k$ is the wavelength, and $\lambda_c = 3.412a$ is the cutoff wavelength for the cylindrical waveguide of radius a. The fields leaking out of the slot are proportional to

$$\int_0^L A(z)e^{-jkz(p-\cos\theta)}dz \tag{2.3}$$

The z-dependence of A(z) arises from the non-uniform gap width along the tapered slot apertures. The integral has its maximum value when $p = \cos\theta$. For $\lambda << \lambda_c$, which occurs when the radius of the cylindrical opening is much greater than the wavelength, θ is approximately 0°, and the radiation is primarily in the forward direction.

Analysis of Diffraction from Tapered Conductor Tips

We have already stated that fields diffracted from tips or corners fall off with distance r as r^{-1}, while edge diffraction decays only as $r^{-1/2}$. Thus, particularly in the far field, one would expect edge diffracted fields to be stronger than those diffracted from tips. However, this is only strictly correct for wavelengths small compared to strip spacing. Using expressions from [6] for electric field intensities from corner and edge diffraction and applying them to our particular problem, we can form the ratio of the field diffracted from the tapered conductor tip to the field diffracted from the edge of the conical horn. The resulting expression is very complicated, involving the sum of two Fresnel integrals. For our conical horn of radius a = 25 cm and half angle $\phi_0 = 20°$, the ratio is much less than unity. Thus the diffraction from the horn edge at the high limit, is much greater than diffraction from the tip.

Note that a particular incident ray originating at the apex of the horn is incident upon the horn edge at an angle of 90°. The "cone" of edge-diffracted rays is, in this case, a plane containing the incident ray and the axis of the horn. One of the diffracted rays in that plane will pass through an observation point located in the same plane. Other incident rays also impinge upon the horn edge at 90°, but their planes of diffracted rays do not pass through the same observation point. Tips, however, diffract rays into 4π steradians. Thus, diffraction from many different tips can contribute to the tip-diffracted component of the field at the observation point, some interfering constructively, others destructively.

Diffraction from Tips of Tapered Slots

The tips of the tapered slots also diffract the incident wave. Slot tip diffraction can be quantified by applying a duality principle to its complementary structure. The two Fresnel integrals, in this case, are subtracted rather than summed and are, in fact, equal for the backlobe direction, resulting in zero slot tip diffraction in that direction. The only contributions to the resultant field at an observation point in the backlobe direction from slot tip diffraction result from diffraction from slot tips not in the incident plane containing the horn axis and observation point. As with the conductor tips, diffracted rays from some ray pairs interfere constructively, and others interfere destructively at the observation point.

2.3 USE OF ABSORBER MATERIALS AROUND ANTENNA

The use of absorber materials around the antenna, as illustrated in Fig. 2.6, is an alternative technique to reduce backlobe and sidelobe emission. The objective is to reduce the sidelobe and backlobe fields with minimal impact upon the forward pattern.

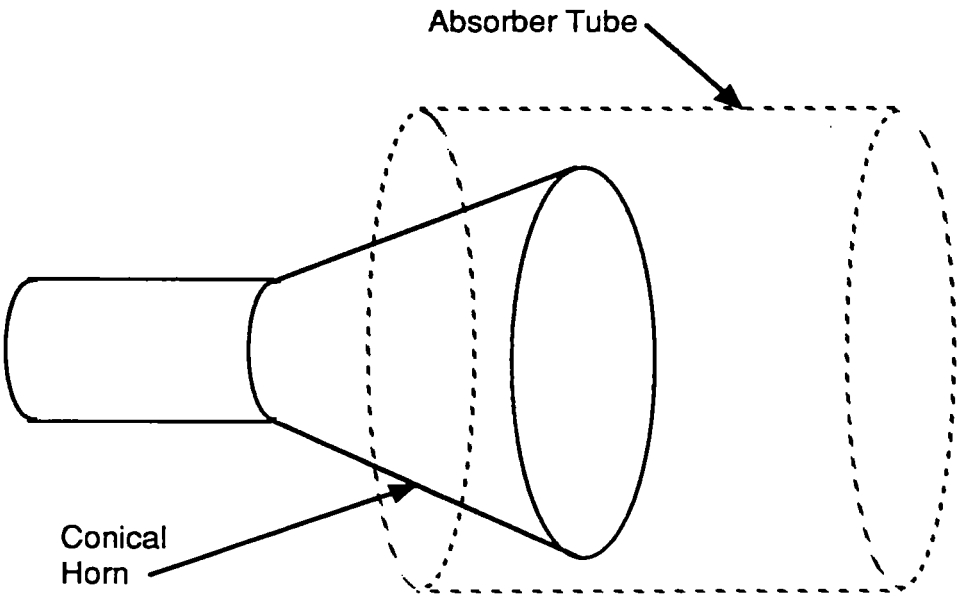

Figure 2.6. Absorber tube over antenna to reduce sidelobes and backlobes.

Peters and Rudduck [4] discuss measurements and theoretical analyses of the use of radar absorbing materials to reduce far sidelobe or backlobe radiation from three basic antenna types: the pyramidal horn, the parabolic reflector, and the Luneberg lens antenna. The authors measured reduction of 10 dB over 100 degrees in the E-plane backlobe radiation for a 14 inch reflector operating at X-band. For a pyramidal horn operating in the TE_{10} waveguide mode the two edges perpendicular to the E-plane produce the diffracted field; the edges perpendicular to the H-plane produce no diffraction because their diffraction coefficients vanish. Experiments with application of absorber to the edges perpendicular to the E-plane of an X-band horn 13.5 in in length with a 9 in x 9 in aperture resulted in approximately 10 dB reduction in the E-plane backlobe. Shielding the edges perpendicular to the H-plane had no effect.

3.0 CALCULATION OF FIELDS FROM TE_{11} HORN

3.1 INTRODUCTION

In this section we will calculate the backlobe fields and gain pattern from a conical horn and compare it with laboratory measurements. Then, in Section 4 we will consider the modifications to the gain pattern with several different cylindrical absorbing hoods placed over the horn.

The radiated fields from an aperture can be calculated accurately by the aperture field method if the linear dimensions of the aperture are at least three-quarters of a wavelength [9, 10]. In the method, the aperture fields are taken to be the incident fields of a feeding waveguide and the radiated fields are calculated by the (vector) Huygens principle, namely,

$$\mathbf{H} = \nabla \times \int_A \hat{\mathbf{n}}' \times \mathbf{H}_a \frac{e^{-jkR}}{4\pi R} dS' - \frac{1}{j\omega\mu} \nabla \times \nabla \times \int_A \hat{\mathbf{n}}' \times \mathbf{E}_a \frac{e^{-jkR}}{4\pi R} dS'$$
$$\mathbf{E} = \frac{1}{j\omega\mu} \nabla \times \mathbf{H} \tag{3.1}$$

where $R = |\mathbf{r} - \mathbf{r}'|$, $\mathbf{r}$ is an observation point, $\mathbf{r}'$ a point in the aperture A, $(\mathbf{E}_a, \mathbf{H}_a)$ are the aperture fields, and $\hat{n}'$ is the unit normal pointing into the region containing the observation point.

The fields of the TE_{11} mode of a cylindrical geometry (see fig. 3.1) are given by [9]

$$H_z = \kappa^2 \cos\phi \, J_1(\kappa\rho) \, e^{-j\beta z}$$
$$H_\rho = -\frac{\beta}{\omega\mu} E_\phi = -j\kappa\beta \cos\phi \, J_1'(\kappa\rho) \, e^{-j\beta z}$$
$$H_\phi = \frac{\beta}{\omega\mu} E_\rho = -j\beta \sin\phi \, \frac{J_1(\kappa\rho)}{\rho} \, e^{-j\beta z} \tag{3.2}$$
$$E_z = 0$$

where $\beta = \sqrt{k^2 - \kappa^2}$, k = free-space propagation constant, $\kappa a = 1.841$, $J_1'(\kappa a) = 0$, a = radius of the aperture. Substituting (3.2) for $\mathbf{E}_a$ and $\mathbf{H}_a$ in (3.1) and evaluating the integral in the far zone (i.e., $r > 2D^2/\lambda$, $D = 2a$), one obtains [9]

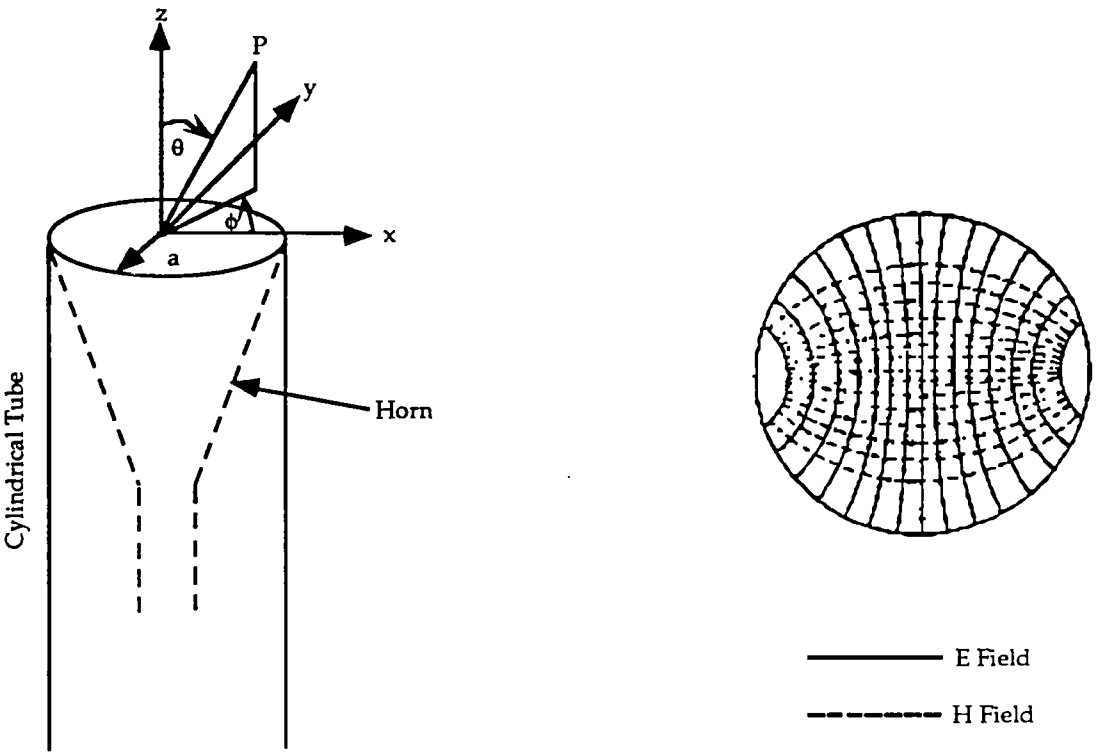

Figure 3.1. Geometry of the problem and the E & H field distributions of the TE11 mode over a cross section.

$$E_\theta = -\frac{\omega\mu}{2}\left(1+\frac{\beta}{k}\cos\theta\right)J_1(\kappa a)\frac{J_1(ka\sin\theta)}{\sin\theta}\sin\phi\,\frac{e^{-jkr}}{r}$$

$$E_\phi = -\frac{ka\omega\mu}{2}\left(\frac{\beta}{k}+\cos\theta\right)\frac{J_1(\kappa a)\,J_1'(ka\sin\theta)}{1-\left(\frac{k\sin\theta}{\kappa}\right)^2}\cos\phi\,\frac{e^{-jkr}}{r} \qquad (3.3)$$

Note that this expression is a very good approximation for all values of θ and ϕ, including θ = 180° since the surface currents on the exterior of the waveguide and higher order mode fields in the aperture can be neglected, provided that the aperture diameter is a wavelength or greater [9].

3.2 DIRECTIVITY AND GAIN

The directivity gain function G is defined as

$$G = 4\pi r^2 \times \frac{1}{2}\,\mathrm{Re}\,(E\times H^*)/P_t \qquad (3.4)$$

where P_t is the total power radiated from the aperture, which can be calculated by integrating the Poynting vector over the aperture, yielding the result [9]

$$P_t = \frac{\pi}{4}\beta\omega\mu\left[(\kappa a)^2 - 1\right] J_1^2(\kappa a) \tag{3.5}$$

Using (3.3) and (3.5) in (3.4), one has

$$G = \frac{0.84(ka)^2}{\beta/k}\left\{\left[\left(1+\frac{\beta}{k}\cos\theta\right)\frac{J_1(ka\sin\theta)}{ka\sin\theta}\right]^2 \sin^2\phi + \left[\left(\frac{\beta}{k}+\cos\theta\right)\frac{J_1'(ka\sin\theta)}{1-(ka\sin\theta/\kappa a)^2}\right]^2 \cos^2\phi\right\} \tag{3.6}$$

where

$$\beta/k = \sqrt{1-(\kappa/k)^2} \quad \text{and} \quad k > \kappa$$

Figure 3.2 is a plot of E-plane and H-plane radiation patterns computed from (3.6) for frequency = 1 GHz and a = 0.26 m.

The main beam is along the z-axis $(\theta = 0, \phi = 0)$ and the ratio of the backlobe to the main beam is, from (3.6), given by

$$\frac{G(\theta=\pi)}{G(\theta=0,\phi=0)} = \left[\frac{1-\sqrt{1-(\kappa/k)^2}}{1+\sqrt{1-(\kappa/k)^2}}\right]^2 \tag{3.7}$$

which is plotted in fig. 3.3 for frequencies from 0.8 to 1.6 GHz. The ratio varies from – 26 dB to – 39 dB; the main lobe gain is about 14 dB at 1 GHz.

3.3 RELATION TO MEASURED SCATTERING PARAMETERS S_{11} AND S_{21}

The results of this analysis will be compared to scattering parameter (S_{11} and S_{21}) data obtained with a vector network analyzer using a MGL-7 surface B-dot sensor mounted on the cylindrical tube containing the horn (see fig. 3.4). The sensor was oriented to measure the azimuthal B-field or longitudinal current density on the cylinder. Thus, it is necessary to relate the scattering parameter S_{21} to the horn gain.

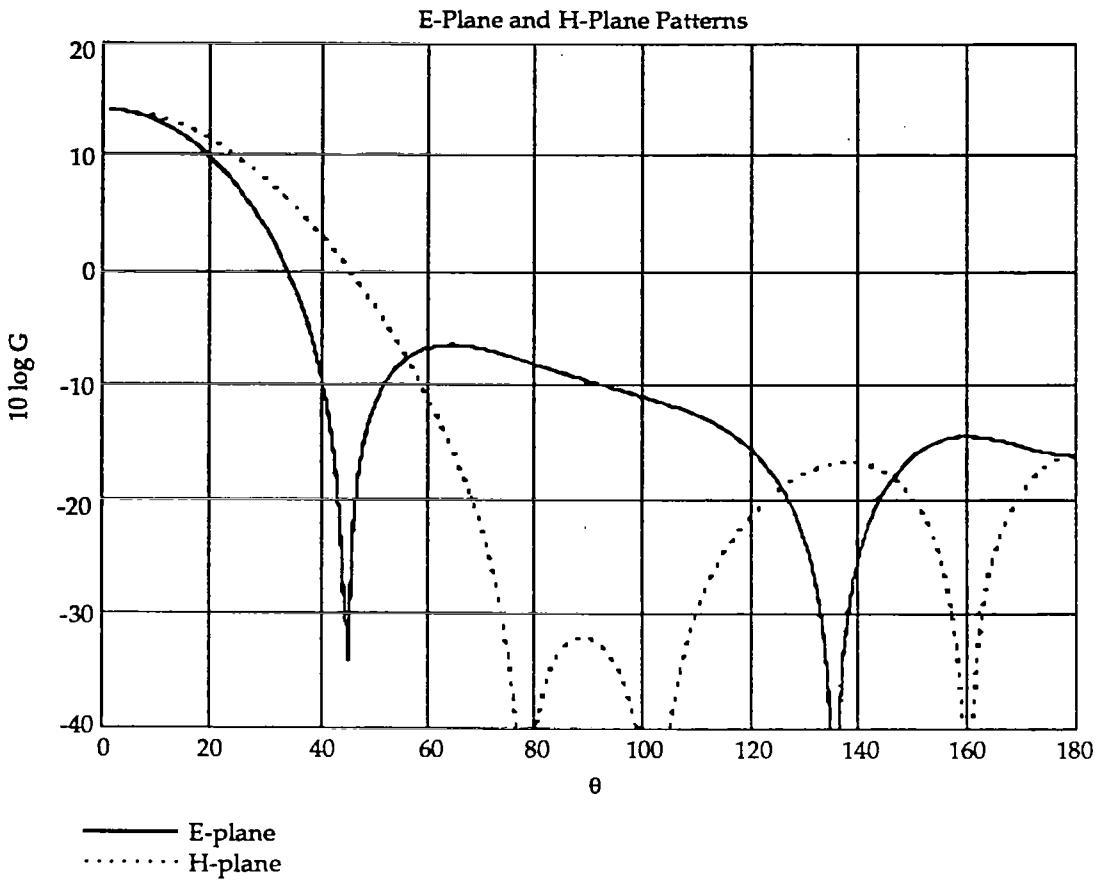

Figure 3.2. E-plane and H-plane radiation patterns calculated from (3.6) for f = 1 GHz and a = 0.26 m.

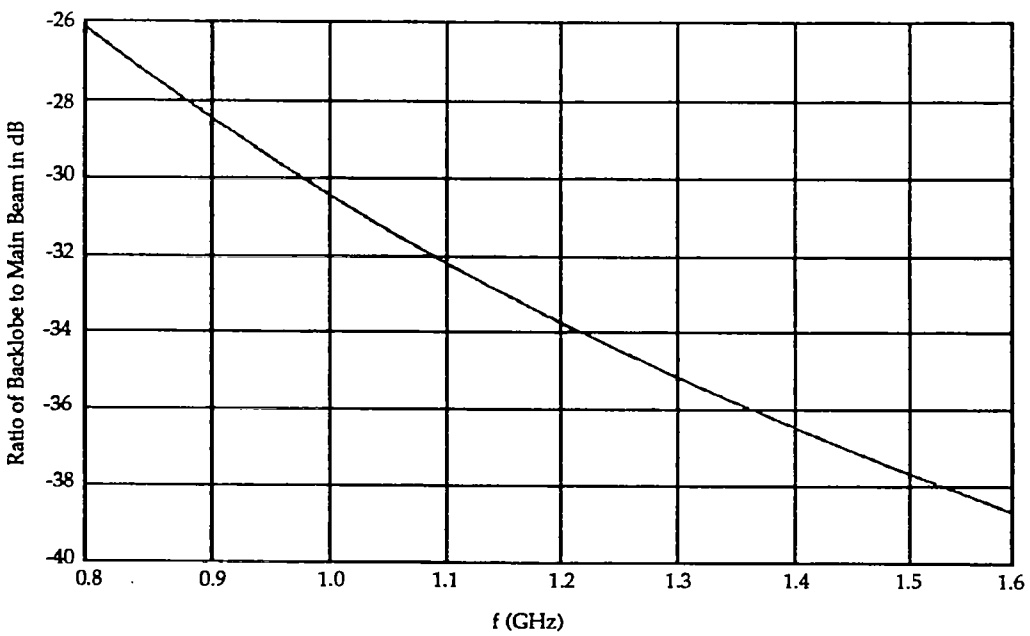

Figure 3.3. Ratio of backlobe to main beam gains for horn antenna as a function of frequency.

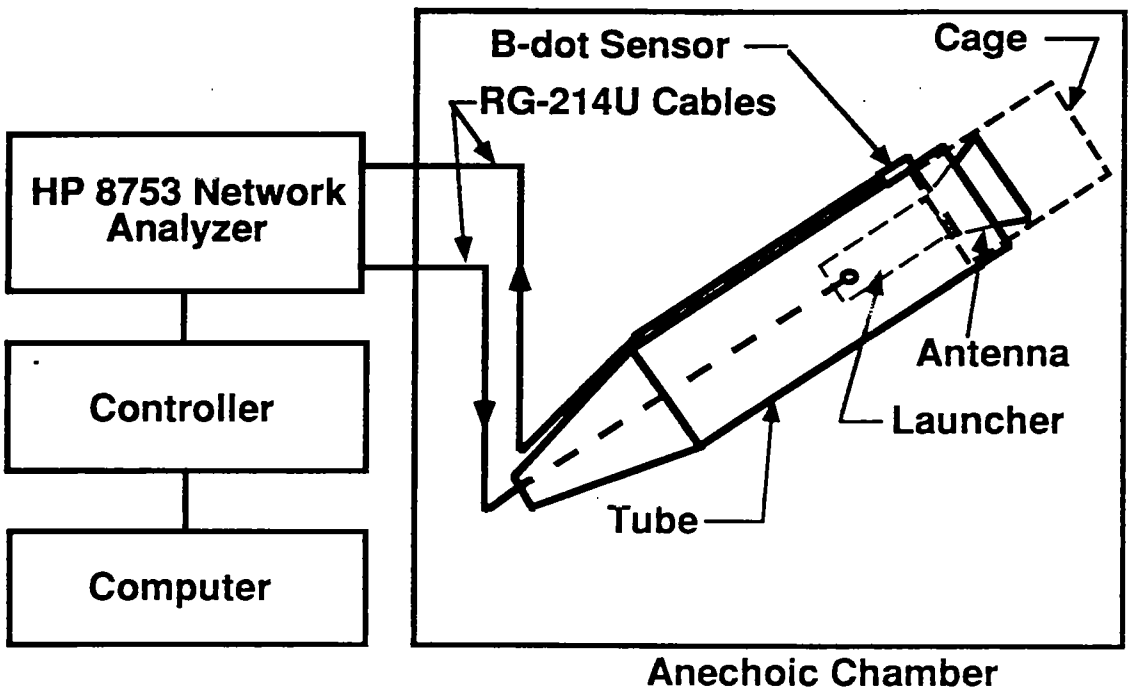

Figure 3.4. Scattering parameter measurements with a B-dot sensor on the cylindrical tube.

The probe has an equivalent area of 1×10^{-4} m^2. The power received by the probe is

$$P_r = \frac{1}{2}\frac{|V|^2}{R} = \frac{1}{2R}(\omega\mu|H_s|A)^2 \tag{3.8}$$

implying that

$$|H_s|^2 = P_r \frac{2R}{(\omega\mu A)^2} \tag{3.9}$$

where R is the load resistance (50 ohms), and H_s is the surface magnetic field, which is twice the incident magnetic field. On the other hand, the directive gain G, expressed in terms of the "incident" field H_{inc}, is

$$G = 4\pi r^2 \times \frac{1}{2} Z_o |H_{inc}|^2 / P_t$$

$$= \pi r^2 \frac{Z_o R}{(\omega\mu A)^2} \frac{P_r}{P_t} = \pi r^2 \frac{Z_o R}{(\omega\mu A)^2} \cdot \frac{|S_{21}|^2}{1-|S_{11}|^2} \tag{3.10}$$

where the definitions $P_t \equiv P_{inc}\left(1-|S_{11}|^2\right)$ and $|S_{21}|^2 \equiv P_r / P_{inc}$ have been used. Using A = 10^{-4} m^2, R = 50 ohms, and the free space impedance $Z_o = 120\,\pi$ ohms, one has, from (3.10),

$$\frac{|S_{21}|^2}{1-|S_{11}|^2} = \frac{1.05}{r^2} \times 10^{-5} \times G f^2 \tag{3.11}$$

or

$$S_{21}(dB) \approx 10 \log\left(\frac{1.05}{r^2}\right) + 10 \log\left(G \cdot f^2\right) - 50 \tag{3.12}$$

where r is the distance from the observation point to the center of the aperture in meters, f is in GHz, and $|S_{11}|$ is assumed to be negligible, consistant with the assumption used in calculating the radiated fields. It is to be noted that, strictly speaking, r must be greater than $2D^2/\lambda$ for (3.10) through (3.12) to be valid. Although the distance of the B-dot probe to the center of the aperture violates this condition in some cases, (3.12) will still be used to calculate S_{21} for comparison with measurements. Figure 3.5 is a plot of 10 log (Gf^2) –50, where G is evaluated at $\theta = \pi$ (backlobe). It is seen that this function varies from –66 dB to – 67 dB over the frequency range 0.8-1.6 GHz.

Figure 3.6 shows the measured S_{21} values at various distances d from the edge of the horn antenna. Note that $r^2 = d^2 + a^2$, where a = 0.26 m is the horn aperture radius. Table 1 summarizes the comparison of calculations based on (3.12) and the measured values.

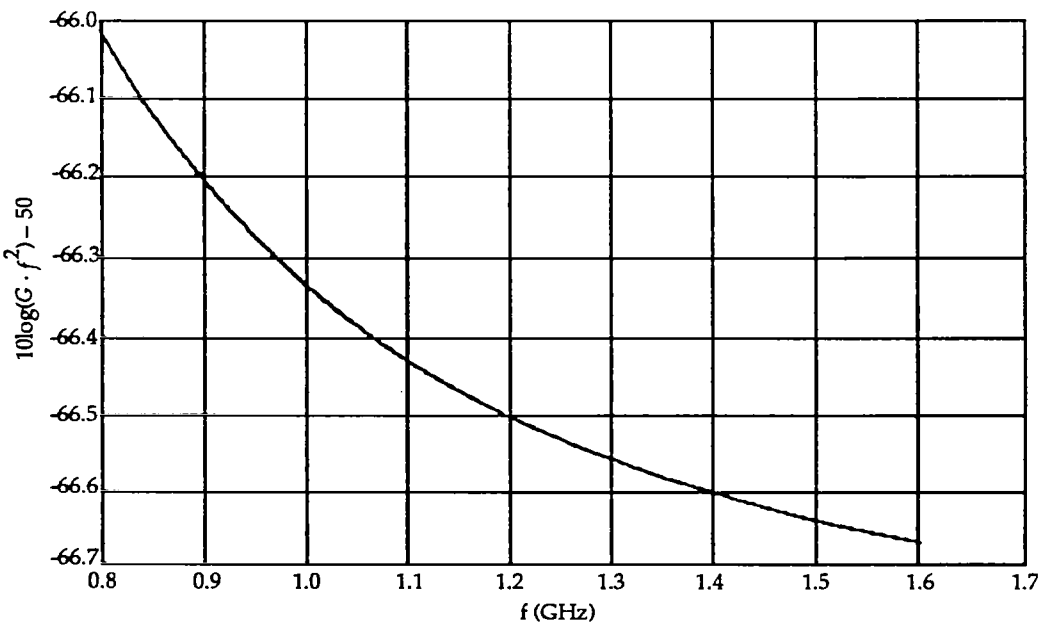

Figure 3.5. Plot of 10 log (Gf^2)-50 vs f with G evaluated at $\theta = \pi$.

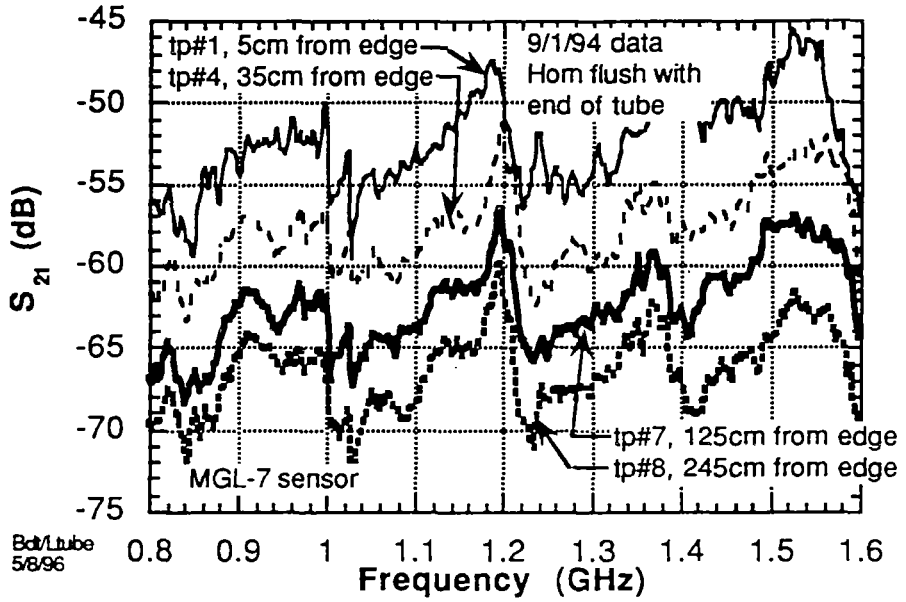

Figure 3.6. Plot of S_{21} vs frequency measured with B-dot sensor on tube oriented to measure B_θ at various distances from the tube edge.

Table 1. Comparison of Calculated and Measured S_{21} Values.

d(m)	S_{21} Calculated from (3.12) (dB)	Measured S_{21} (dB)
0.05	-54	-53
0.35	-59	-58
1.25	-68	-64
2.45	-74	-68

The agreement seems to be better for closer distances, even though (3.12) is valid only in the far field. The test data indicate two other surprising features: the measured signals do not decay as $1/r^2$ for the greater distances (e.g., from 1.25 m to 2.45 m), and they drift slowly upward at higher frequencies. This may be due to the fact that the tube exterior has a constant radius, not increasing as a cone, which may better exhibit the $1/r^2$ behavior.

The locations of the measured signal peaks shown in Fig. 3.6 can be explained in terms of the length resonances of the 1.83 m long cylindrical tube on which the sensor was mounted. The resonance frequencies of the tube are given by

$$f_n = \frac{2n+1}{2} \cdot \frac{c}{L}, \quad n = 0, 1, 2 \ldots \tag{3.13}$$

where L = length of the tube and c = speed of light in free space. The spacing between two succesive resonance frequencies is calculated to be

$$f_{n+1} - f_n = \frac{c}{L} = \frac{3 \times 10^8}{1.83} = 0.164\, GHz \tag{3.14}$$

which is in fairly good agreement with fig. 3.6.

4.0 CALCULATION OF FIELDS WITH BACKLOBE SUPPRESSION DEVICE

4.1 INTRODUCTION

This section examines ways of employing absorber materials to reduce side- and back-lobe emissions from a conical horn. We begin by considering a cylindrical hood of absorbing material wrapped around the radiating horn. Then we consider the same hood with periodic, rectangular, longitudinal notches.

4.2 CYLINDRICAL ABSORBING HOOD

Figure 4.1 shows S_{21} data acquired with an MGL-7 B-dot sensor located at 0.35m from the edge of a cylindrical tube of Emerson Cumings LS-26 absorber foam material, approximately 1/2 in thick. The radiating horn extends about 0.2 m (8") outside the tube, as illustrated in the inset. Thus, the distance r_0 from the center of the horn aperture to the location of the sensor (referred to as "TP #4") is

$$r_0 = \sqrt{(0.26)^2 + (0.55)^2} = 0.61m. \tag{4.1}$$

The S_{21} values predicted by (3.12) with no hood, with $\theta = \pi$ and $r = r_0 = 0.61$ m, are between -62.5 dB and -61.5 dB *for* $0.8 \le f(GHz) \le 1.6$, while the average measured values are about −60 dB for the no-hood case.

With the cylindrical hood of absorbing material attached as illustrated in fig. 4.1, S_{21} at the same test point (i.e., TP #4) is expected to be lower for two reasons:

- the radiating aperture is farther away from TP#4, and
- the power available for radiation is less because some power is lost to the absorbing material.

LS-26 absorber foam material has a surface resistance about 47 ohms per square and a corresponding skin depth at 1 GHz of about 1.2 cm, which is approximately the thickness of the absorber material used to construct the hood.

Since the length of the hood beyond the edge of the tube is about 0.48m (or 19"), the distance of the B-dot sensor from the center of the radiating aperture is now

$$r = \sqrt{(0.26)^2 + (1.03)^2} = 1.06m \tag{4.2}$$

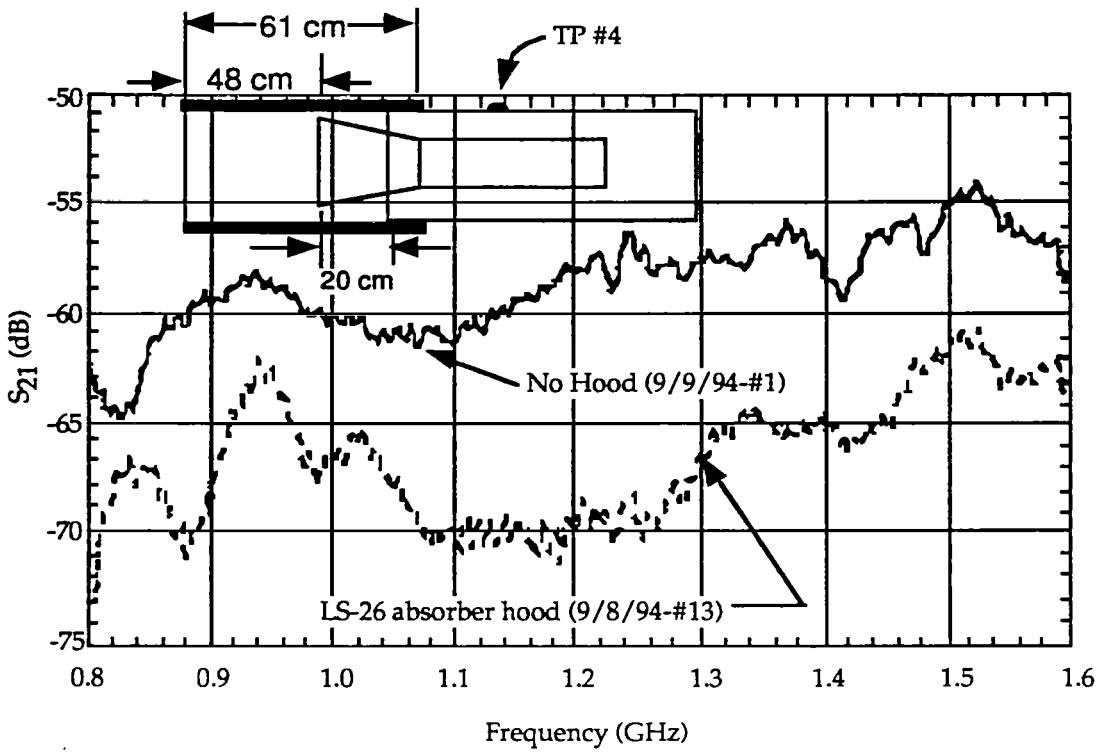

Figure 4.1. S_{21} data vs frequency measured at test point #4 with a cylindrical hood of LS-26 foam absorber around the horn.

Thus, the expected reduction in S_{21} from the baseline case (no hood) is

$$10 \log\left(\frac{0.61}{1.06}\right)^2 = -4.8\,dB \tag{4.3}$$

Next, the power lost to the LS-26 foam will be computed. The time-average power absorbed is

$$P_{abs} = \int_o^L \int_o^{2\pi} \frac{1}{2} R_s \left(|H_\phi|^2 + |H_z|^2\right) a\, d\phi\, dz \tag{4.4}$$

where L = length of the hood, and R_s is the surface resistance. Using (3.2) for H_ϕ and H_z in (4.4) and evaluating the integrals one obtains

$$P_{abs} = \frac{\pi}{2} R_s L a \left[\beta^2 \frac{J_1^2(\kappa a)}{a^2} + \kappa^4 J_1^2(\kappa a)\right]. \tag{4.5}$$

Thus, the ratio of power loss to the total power radiated in the no-hood case is

$$\frac{P_{abs}}{P_t} = 2 \cdot \frac{R_s}{Z_o} \cdot \frac{L}{a} \cdot \frac{1}{(\beta a)(ka)} \cdot \frac{(\beta a)^2 + (\kappa a)^4}{(\kappa a)^2 - 1} \tag{4.6}$$

where (3 -5) has been used for P_t.

Let us define an efficiency η as

$$\eta = 1 - \frac{P_{abs}}{P_t} \tag{4.7}$$

Using $R_s = 47\sqrt{f}\ \Omega$ (f in GHz), $L = 0.48m$, $a = 0.26$m one finds that

$$-1.3 \geq \eta\ (\text{dB}) \geq -1.4 \tag{4.8}$$

for $0.8 \leq f(GHz) \leq 1.6$. Thus the loss due to absorption by the 0.48 m long hood of LS-26 foam is only −1.4 dB for the frequency range of interest.

Adding the losses computed in (4.3) and (4.8), one obtains about −6.2 dB reduction from the no-hood case, which agrees well with measurements (about −7 dB average), as shown in fig. 4.1.

4.3 CYLINDRICAL ABSORBING HOOD WITH NOTCHES

In the preceding subsection it was seen that absorption in a cylindrical absorbing hood would reduce backlobe radiation by only about 1.4dB. (The other 4.8dB reduction results from moving the radiating aperture farther away from the MGL-7 sensor.) To have further reduction one has to think of using other schemes. One such scheme is shown in fig. 4.2 where longitudinal slots are cut in the absorbing hood, resulting in a cage of rectangular slats of absorber material separated by rectangular gaps which function like an array of notch antennas.

Figure 4.3 shows a notch antenna in a half-plane sheet and its complementary strip monopole sitting on the edge of a half-plane sheet. When the length h of the notch is an odd multiple of a quarter wavelength, the notch antenna radiates efficiently into the forward direction. When the length is an even multiple of a quarter wavelength, it will hardly radiate at all.

It is known [9, 11] that the radiation conductance G and susceptance B of a notch antenna are given by

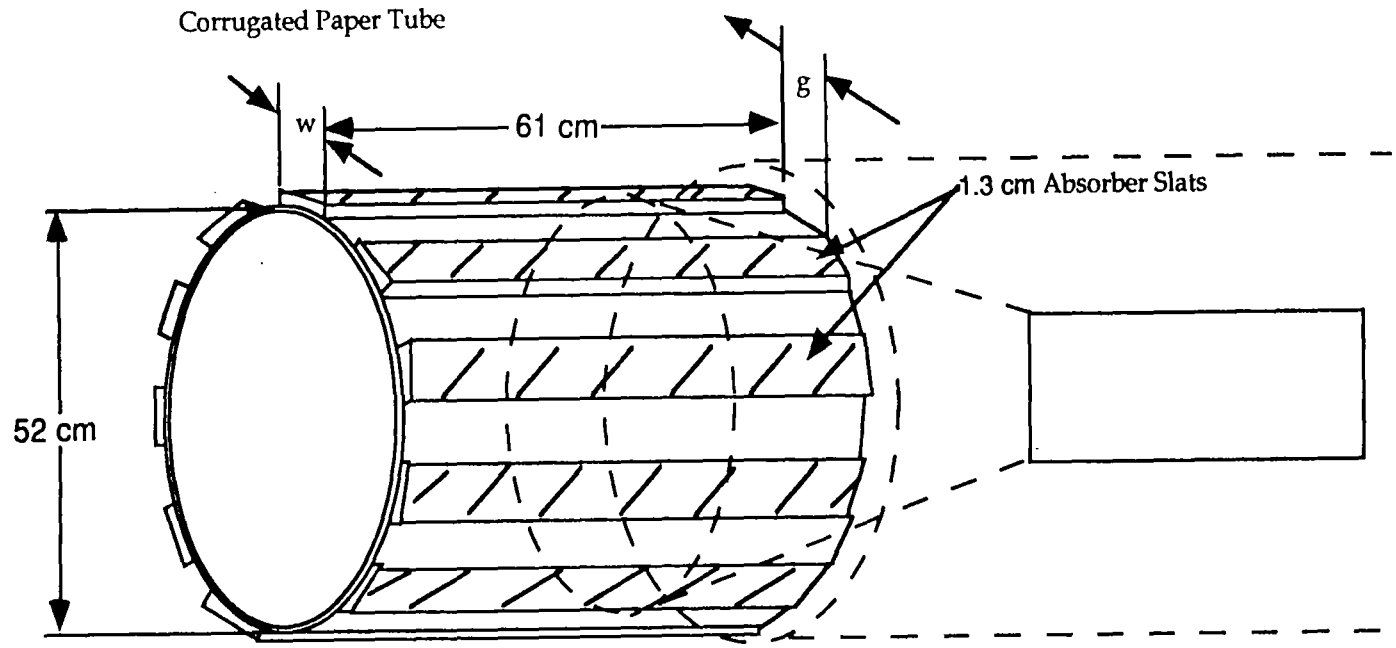

Figure 4.2. Absorber tube with longitudinal slots over a conical horn antenna.

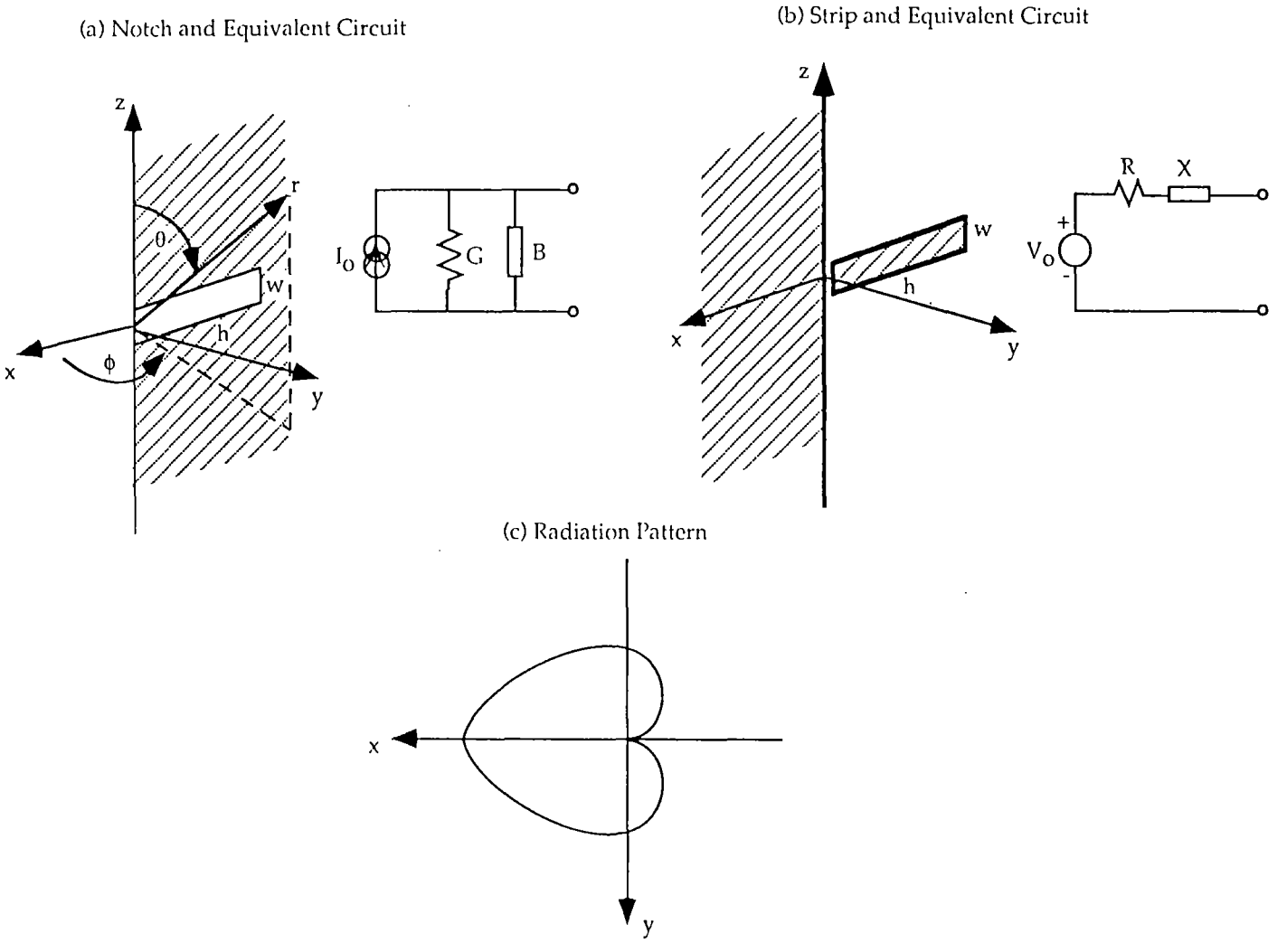

Figure 4.3. Notch antenna, its complementary monopole on a half-plane sheet, and radiation pattern on the z = 0 plane of a quarter-wavelength notch.

$$G = \frac{3}{2Z_o}\left[C(kh) - \cot(kh)\cdot S(kh)\right]^2 \tag{4.9}$$

$$B = jY_c \cot(kh) \tag{4.10}$$

where

$$Y_c = \frac{2}{\pi Z_o}\left[\ell n(16h/w) - 1\right] \tag{4.11}$$

and where C(x) and S(x) are Fresnel cosine and sine integrals defined as

$$C(x) = \int_o^x \frac{\cos t}{\sqrt{2\pi t}}\, dt \qquad S(x) = \int_o^x \frac{\sin t}{\sqrt{2\pi t}}\, dt \tag{4.12}$$

Referring to the equivalent circuit of a notch antenna (fig. 4.3a), the time-average radiated power is

$$P_{rad} = \frac{1}{2}\,\frac{G}{G^2 + |B|^2}\,|I_o|^2 \equiv \frac{1}{2}\,R_r\,|I_o|^2 \tag{4.13}$$

The quantity R_r is plotted vs. kh and f(GHz) in figs. 4.4 and 4.5, respectively, for slot height to width ratio h/w = 4.7 (h = 35 cm and w = 7.4 cm), corresponding to a 11 slat/11 notch cage like the one tested. It can be seen that the peaks of R_r occur at kh = $\pi/2$, $3\pi/2$, $5\pi/2$, $7\pi/2$, etc., corresponding to h = (2n+1) $\lambda/4$, where n = 0,1,2.... Thus, for a given notch length h, the maxima for radiation occur at frequencies given by

$$f_n = (2n+1)\frac{c}{4h}, \quad n = 0,1,2,... \tag{4.14}$$

The spacing between two successive resonance frequencies is

$$f_{n+1} - f_n = \frac{c}{2h}. \tag{4.15}$$

Figure 4.6 shows plots of S_{21} versus frequency for the 11-slat/notch cage for slat lengths h = 35 cm (14") and 33 cm (13") extending from the horn aperture. Using (4.14) to calculate the first four resonance frequencies, one obtains the results shown in Table 2. Also shown are the corresponding frequencies at which measured values of S_{21} are at a null in fig. 4.6. The agreement between calculations and measurements appears to be quite good.

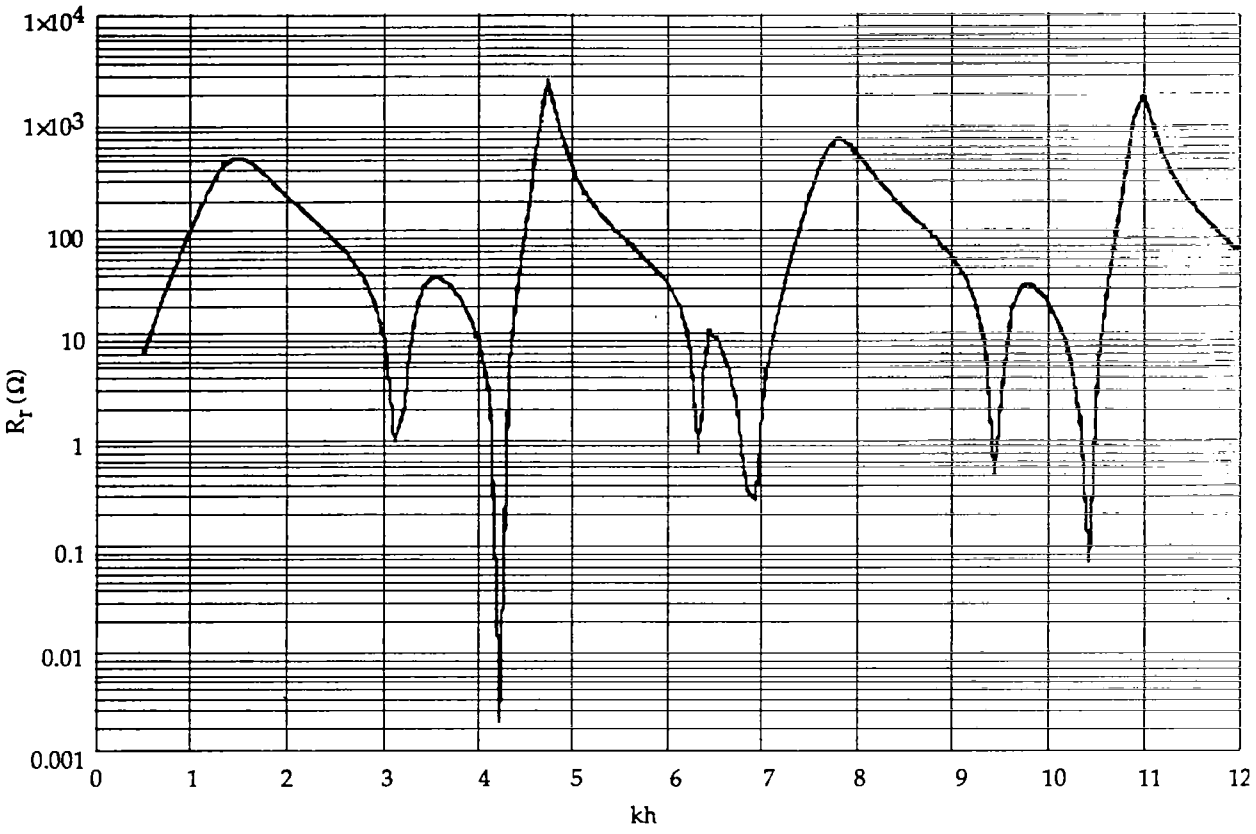

Figure 4.4. Plot of radiation resistance R_r vs kh for h/w=4.7.

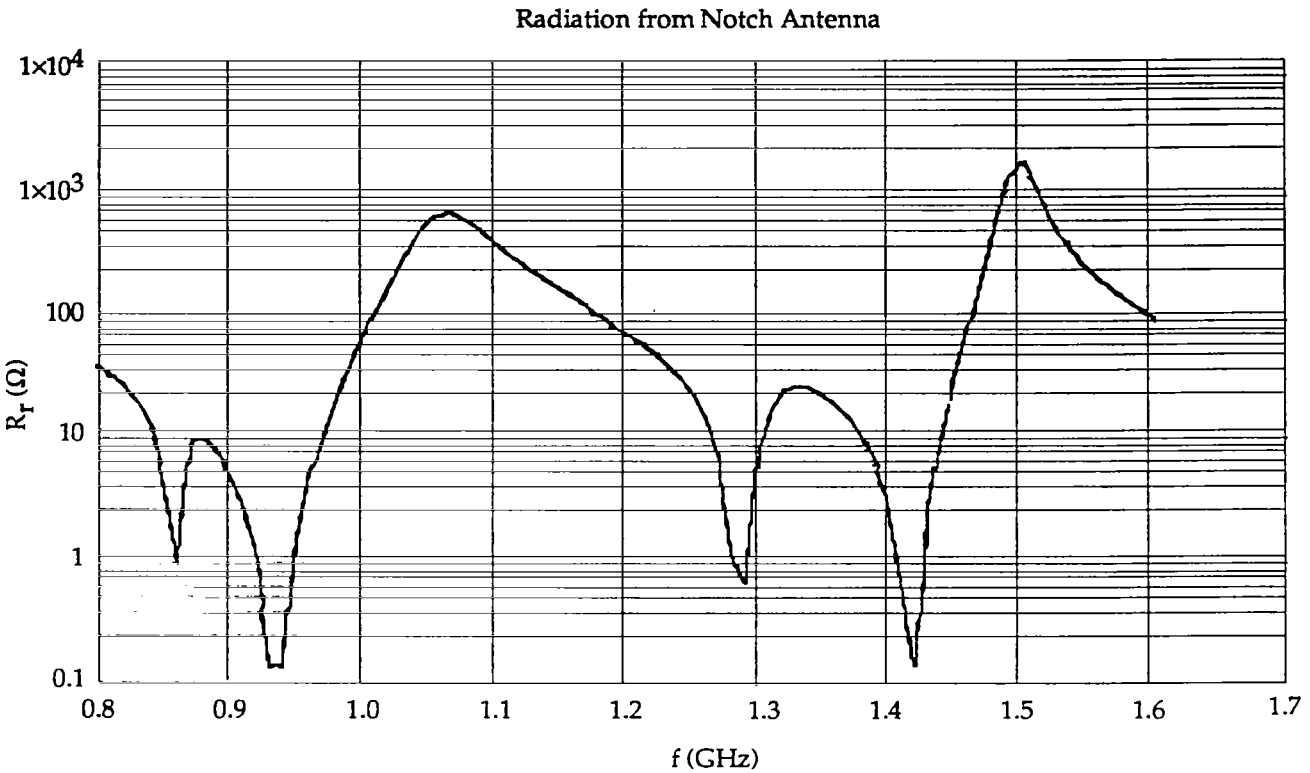

Figure 4.5. Plot of radiation resistance R_r vs f for h/w=4.7.

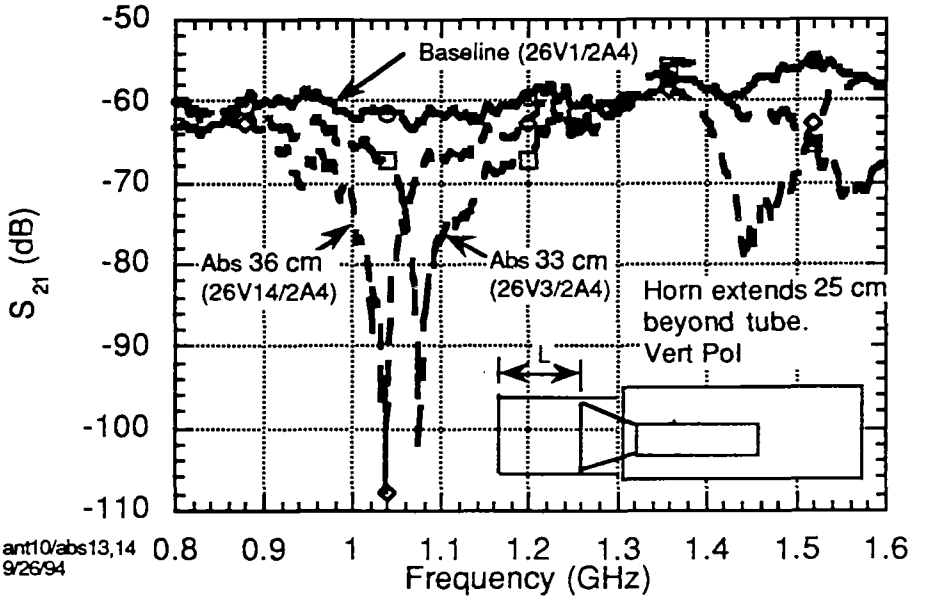

Figure 4.6. Test point #4 S_{21} signal vs frequency with 11-slat cage extending 33 cm and 36 cm beyond the edge of the horn.

We now calculate the S_{21} parameter. (3.12) can be re-written as follows:

$$S_{21}(dB) = 10\log\left(\frac{1.05}{r^2}\right) + 10\log\left(Gf^2\right) - 50 + 20\log\left(\frac{\eta_0}{r}\right) + 10\log\eta \tag{4.16}$$

Table 2. Comparison of Notch Resonances and Measurement Nulls.

	h = 35 cm (14in)		h = 33 cm (13in)	
n	Notch Resonance Frequency (GHz)	S_{21} Measurement Null (GHz)	Notch Resonance Frequency (GHz)	S_{21} Measurement Null (GHz)
0	0.21	-	0.23	-
1	0.64	-	0.68	-
2	1.07	1.04	1.14	1.1
3	1.50	1.46	1.59	1.56

where the distance r_0 from the sensor location to the center of the horn aperture was calculated in (4.1) to be 0.61 m. The first three terms of (4.16) give the value of S_{21} for the baseline configuration, and the last two terms represent, respectively, the reduction due to increased distance r from the aperture and to a combination of absorption loss and radiation loss from the notches (accounted for in the efficiency factor η).

For the case where the slats are 0.35 m (or 14") long, r ≈ 0.94 m, one has

$$20\log\left(\frac{r_o}{r}\right) = 20\log\left(\frac{0.61}{0.94}\right) = -3.76\,dB, \tag{4.17}$$

Thus, the reduction in S_{21} from the baseline configuration due to the increased distance is 3.76 dB.

To calculate η one first calculates the radiation loss from the notches and then the absorption by the LS-26 slats. Since G and B for the notch were already determined in (4.9) and (4.10), one only needs to calculate I_o for (4.13). As shown in fig. 4.3, I_o is the current at the "mouth" of the notch driving the notch antenna and is thus related to the product of the notch width w and H_z at the mouth (i.e., $I_0 = 2w\,H_z$). If H_z is taken to be the z-component of the H-field of the TE_{11} mode (see (3.2)), one then has

$$\frac{|I_o|^2}{P_t} = \frac{|2w\,H_z|^2}{P_t} = \frac{4}{P_t}\,w^2\kappa^4\cos^2\phi\;J_1^2(\kappa a) \tag{4.18}$$

where P_t is the total radiated power in the baseline case and is given by (3.5). Since there are as many notches as slats, the integral of $\cos^2\phi$ over all notches will be $\pi/2$. Hence (4.18) becomes

$$\frac{|2w\,H_z|^2}{P_t} = \frac{8}{Z_o}\left(\frac{w}{a}\right)^2\frac{(\kappa a)^4}{(\kappa a)^2-1}\,\frac{1}{\beta a\cdot ka}$$

$$= \frac{2.808\times10^{-4}}{f^2\sqrt{1-(0.338/f)^2}} \qquad (f\ in\ GHz) \tag{4.19}$$

Assuming each of the 11 notches radiates incoherently, the total power loss, P_{rad}, due to radiation from the notches with respect to the total power P_t available for radiation in the baseline case is (see (4.13))

$$\frac{P_{rad}}{P_t} = \frac{1}{2} R_r \frac{|2w H_z|^2}{P_t} \times 11$$

$$= \frac{1.544 \times 10^{-3} R_r}{f^2 \sqrt{1-(0.338/f)^2}} \tag{4.20}$$

where R_r has been plotted in fig. 4.4.

It should be remarked here that in the above numerical calculations (viz., (4.19)), the vacuum speed of light c was used. If the phase speed of the TE_{11} mode is used instead, the numerical factor in (4.20) (1.544×10^{-3}) is larger. The phase speed v_{ph} of the TE_{11} mode is given by

$$v_{ph} = \frac{c}{\sqrt{1-(\kappa/k)^2}} = \frac{c}{\sqrt{1-(0.338/f)^2}} \quad (f \text{ in GHz}) \tag{4.21}$$

Thus, in the frequency range of interest, 0.8 to 1.6 GHz,

$$1.02 \leq v_{ph}/c \leq 1.10 \tag{4.22}$$

We will show that a small change in the numerical factor (1.544×10^{-3}) in the numerator of (4.20) can produce a significant change in the depth of the notch at 1.04 GHz in fig. 4.6.

The absorption power loss, P_{abs}, due to the 11 LS-26 slats is simply half of that given in (4.6), since only half the surface is absorber. Setting L = 35 cm (14"), a = 26 cm, and $R_s = 47\sqrt{f}$, one obtains

$$\frac{P_{abs}}{P_t} = 0.070 \frac{(f^2 - 0.114) + 0.389}{\sqrt{f^3 - 0.114 f}} \tag{4.23}$$

Combining (4.20) and (4.23) one obtains for the efficiency factor η:

$$\eta = 1 - \frac{P_{rad}}{P_t} - \frac{P_{abs}}{P_t} = 1 - \frac{1.544 \times 10^{-3} R_r}{f^2 \sqrt{1-(0.338/f)^2}} - 0.070 \frac{f^2 + .275}{\sqrt{f^3 - .114 f}} \tag{4.24}$$

Figure 4.7 is a plot of the reduction in backlobe radiation with the 11-slat absorber cage of 35 cm (14 in) length relative to the baseline case as a function of frequency. This reduction was calculated by subtracting 3.76 dB (the additional loss due to increased distance from the aperture to the sensor as

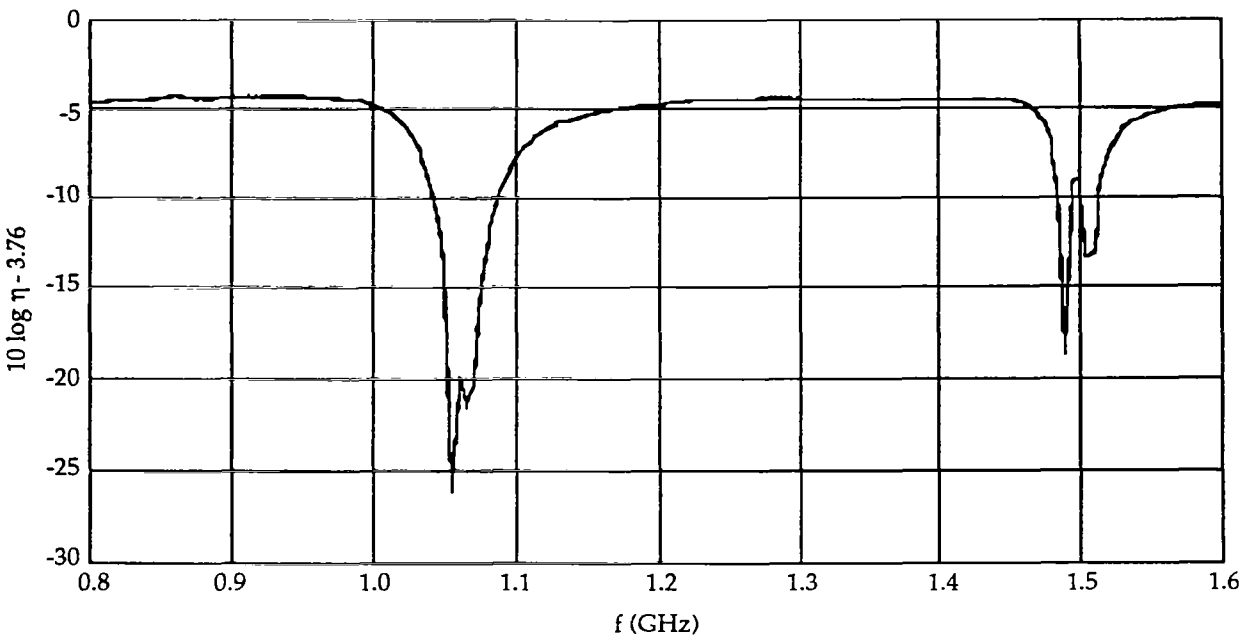

Figure 4.7. Reduction in backlobe intensity vs frequency with the 11-slat absorber cage extending 36 cm beyond the horn edge, calculated from (4.24) with the numerical factor 1.544×10^{-3}.

calculated in (4.17)) from the efficiency factor η calculated from (4.24) and expressed in dB. Since S_{21} for the backlobe sensor for the baseline case is about −62dB (see (4.2)), the expected value for S_{21} with the 14 in long, 11-slat cage attached (for comparison with the measured value in fig. 4.5) is obtained by subtracting 62 dB from the reduction values plotted in fig. 4.6.

Figure 4.8 is the same plot with a 9% change of the numerical factor in (4.24) from 1.544×10^{-3} to 1.680×10^{-3}. It is evident that this slight change can have a large effect on the depth of the resonance around 1.05 GHz. This illustrates the sensitivity of the depths of resonances to the accuracy of the model used. Since the model presented here neglects, among other things, the interaction between notches and the TE_{11} mode fields at the "mouth" of the cage, its accuracy in predicting the depths of the notches is limited. It is indeed somewhat surprising that this approximate model could predict the depths of the resonances as well as that shown in fig. 4.7.

Before concluding, we consider briefly the radiation pattern of a notch in a half-plane sheet. For a notch length h not more than one-third of a wavelength, the far-zone radiated fields have been worked out in the case of a semi-infinite sheet [11]:

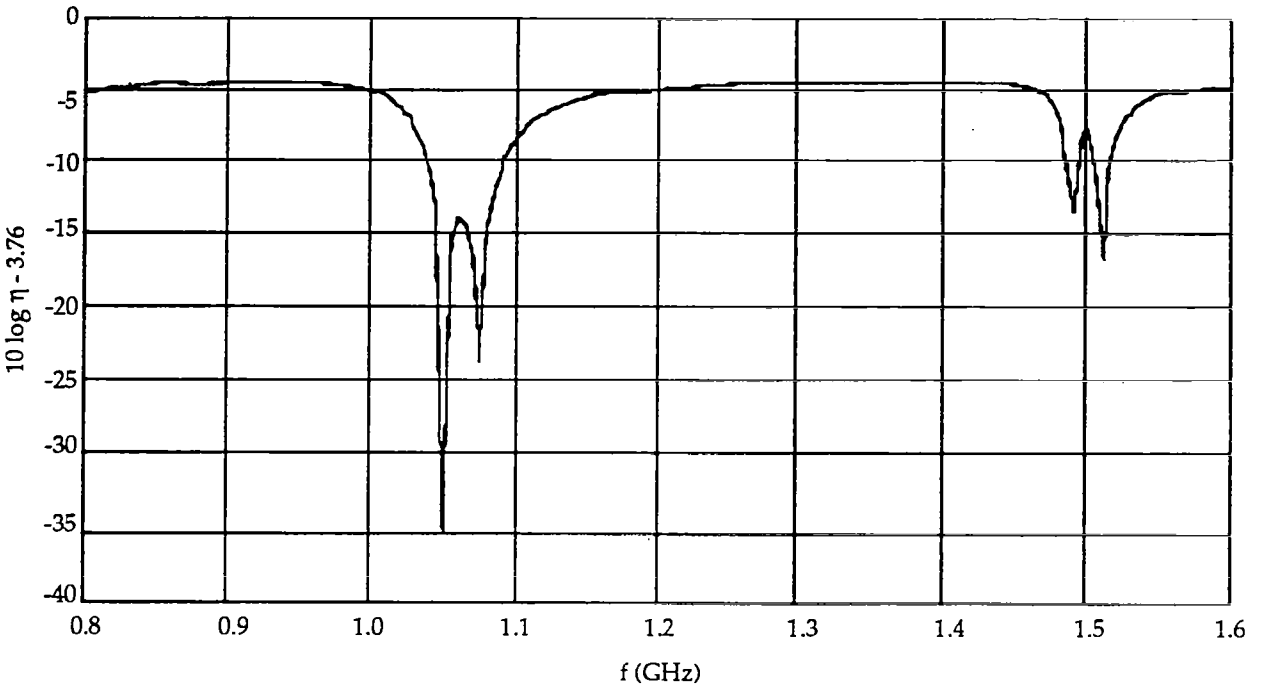

Figure 4.8. Reduction in backlobe intensity vs frequency with the 11-slat absorber cage extending 36 cm beyond the horn edge, calculated from (4.24) with the numerical factor 1.680×10^{-3}.

$$E_\theta = \frac{A}{r}\frac{1}{\sqrt{\sin\theta}}\cos(\phi/2)$$
$$E_\phi = \frac{A}{r}\frac{\cos\theta}{\sqrt{\sin\theta}}\sin(\phi/2) \qquad (4.25)$$

from which the directivity gain function G is found to be

$$G = \frac{4\pi\left(|E_\theta|^2 + |E_\phi|^2\right)}{\int_0^\pi \int_0^{2\pi}\left(|E_\theta|^2 + |E_\phi|^2\right)\sin\theta\, d\theta\, d\phi} \qquad (4.26)$$
$$= \frac{8}{3\pi}\frac{1}{\sin\theta}\left[\cos^2(\phi/2) + \cos^2\theta\sin^2(\phi/2)\right]$$

and the spherical coordinates (r, θ, φ) are defined in fig. 4.3a. On the x-y plane ($\theta = \pi/2$) (4.26) gives

$$G(\pi/2,\phi) = \frac{4}{3\pi}(1+\cos\phi), \qquad (4.27)$$

which is the cardioid pattern as shown in fig. 4.3c. Along the edge of the sheet ($\theta = 0, \pi$), G is infinite due to the assumption of an semi-infinte sheet. If the sheet is of finite extent, G is finite everywhere. This case has been reported in [11] and reproduced in fig. 4.9.

(a) E_θ, E_ϕ in z = 0 plane

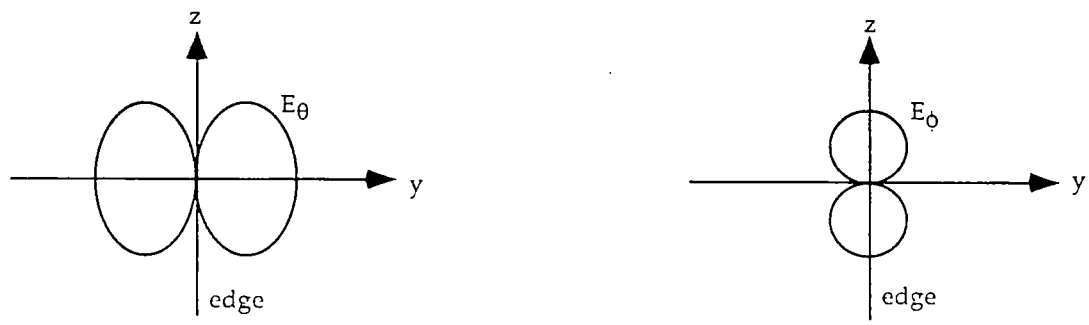

(b) E_θ, E_ϕ in x = 0 plane

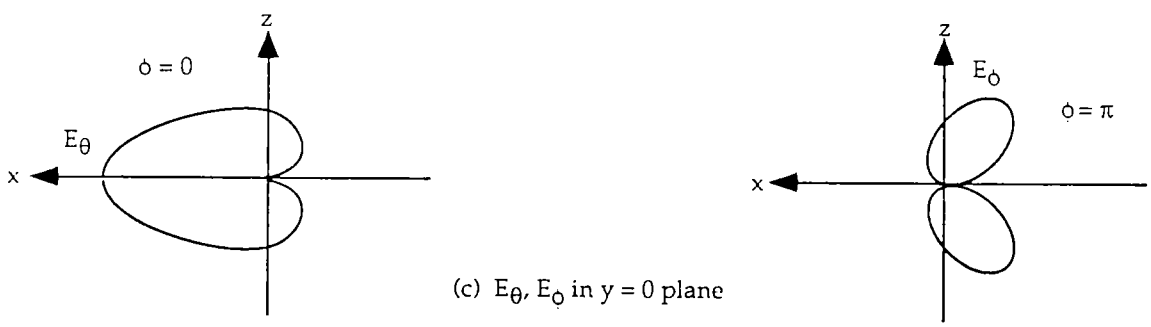

(c) E_θ, E_ϕ in y = 0 plane

Figure 4.9. Field patterns for finite sheet [11].

5.0 SUMMARY AND CONCLUSIONS

This paper has considered techniques for reducing backlobe and sidelobe emissions from a conical horn antenna. We discussed three general techniques which either absorb or re-direct back- and side- lobe emissions:

1.) modification of horn design, particularly the edges, to minimize diffraction,
2.) the use of a cylinder of RF absorber material over the horn.
3.) attachment of a device to re-direct diffracted rays
    3.1 conducting strips
    3.2 tapered conducting strips
    3.3 resistively loaded tapered conducting strips

Dual mode horns, corrugated horns, and aperture matched horns were considered as examples of approach (1). Since the diffracted fields depend on both the edge diffraction coefficient and the magnitude of the field at the edge of the horn, reduction in either can be effective in reducing backlobe emission. Dual mode horns and corrugated horns are designed to reduce the magnitude of the fields at the horn edge, while the aperture matched horn is designed to reduce the magnitude of the edge diffraction coefficient.

In Section 2 we discussed the general implementation of approach (2) using a device consisting of long, tapered strips of conducting material attached to the edge of the horn. By replacing the horn edges, which are normal to the incident rays, by edges nearly parallel to the incident rays, the diffracted rays are re-directed to the forward direction, as can be seen by considering the Keller's cones of edge-diffracted rays. We also discussed the use of tapered strips of absorbing materials either in place of or in addition to the tapered conducting strips to provide a more gradual transition from the horn aperture to free space and thus reduce the standing waves inside the cage of tapered strips. However, the sheet resistance needs to be lowered and experimentally optimized (including shape).

Surrounding the horn with radar absorbing material has been shown in the literature to be an effective way to achieve up to 10 dB reduction in side-lobes and back-lobes from an aperture antenna by simply absorbing RF energy radiated in these directions. Applying radar absorber materials to the aperture edges has also been shown to be as effective.

In Sections 3 and 4 we discussed at some length the implementation of a slotted absorber hood for redirecting side- and back-lobe emissions, i.e. approach (2). The device consists of an array of

rectangular notches around the horn, parallel to the horn axis. Its effectiveness in reducing backlobe emission, compared to that of the horn alone, was demonstrated both analytically and experimentally. We showed that, at a particular frequency, notches with lengths equal to an odd multiple of a quarter wavelength will radiate mainly into the forward direction, augmenting the main lobe radiated by the horn and reducing the radiation into the back lobe but with little effect on the side lobes.. Because it is a resonant structure, it is useful mainly for narrowband applications. The device considered in Section 2 with tapered conducting strips and tapered notches, however, does not depend upon resonance effects and therefore has broadband applicability.

This technique for reducing radiation in unwanted direction is similar in function to an opaque lamp shade. At microwave wavelengths (as compared to optical wavelengths), however, the diffraction at the edge of the shade is much more significant. A microwave shade is greatly improved by treatment of the shade edge as discussed in this paper, with perhaps even further future refinements.

The discussions in this paper were limited to a conical horn antenna, but the concepts presented should apply generally to any aperture antenna, including other horns (pyramidal, TEM, etc.) and reflectors.

REFERENCES

1. P. D. Potter, "A new antenna with suppressed sidelobes and equal beamwidths," *Microwave Journal*, June, 1965.

2. R. E. Lawrie and L. Peters, Jr., "Modifications for horn antennas for low sidelobe levels," *IEEE Trans. Antennas Propagat.*, vol. AP-14, no. 5, pp. 605-610, Sept., 1966.

3. W. D. Burnside and C. W. Chuang, "An Aperture-Matched Horn Design,"

4. L. Peters, Jr. and R. C. Rudduck, "RFI Reduction by Control of Antenna Sidelobes," RADC-TDR-63-133, May, 1963.

5. J. B. Keller, "Diffraction by an Aperture," Journal of Applied Physics, Vol 28, No. 4, pp 426-444, April, 1957.

6. Y. T. Lo and S. W. Lee, *Antenna Handbook: Theory, Applications, and Design*, Van Nostrand REinhold Company, New York, NY, 1988.

7. T. T. Wu and R.W.P. King, "The Cylindrical Antenna with Non-Reflecting Resistive Loading," IEEE Trans. on Antennas and Propagation, AP-13, Nov., 1965.

8. S. Ramo and J. R. Whinnery, Fields and Waves in Modern Radio, Second Edition, John Wiley and Sons, New York, 1953, page 322.

9. S. Silver, Microwave Antenna Theory and Design, MIT Radiation Laboratory Series, vol. 12, McGraw-Hill, New York, 1949.

10. Henry Jasik (editor), Antenna Engineeering Handbook, McGraw-Hill, New York, 1961.

11. W. A. Johnson, "The Notch Aeriel and Some Applications to Aircraft Radio Installations," Proc. IEE (London), pt. B, vol. 102, pp. 211-218, March 1955.